2011 2nd International Conference on Environmental Science and Development
IPCBEE vol.4 (2011) © (2011) IACSIT Press, Singapore

Water quality changes during aquifer storage and recovery: Quantification of water-sediment interactions and reactive transport modeling.

Carlos Descourvieres and Henning Prommer
CSIRO, Land and Water
School of Environmental Systems Engineering
The University of Western Australia
Perth, Australia
e-mail: carlos.descourvieres@csiro.au
Henning.Prommer@csiro.au

Carolyn Oldham
School of Environmental Systems Engineering
The University of Western Australia
Perth, Australia

Janek Greskowiak
Institute for Biology and Environmental Sciences, Carl von Ossietzky University of Oldenburg, Germany

***Abstract*— Incubation experiments were used to study the geochemical controls on sediment reactivity and buffering processes during the injection of oxygen (O_2) saturated reverse osmosis (RO) waters into a deep anoxic heterogeneous siliclastic sedimentary aquifer. Pyrite (20 – 100% reactive), sedimentary organic matter (SOM; 3 – 56%), and siderite (3 – 28%) were the main O_2 reductants. Trace-levels of carbonate acted as a pH buffer, while a lower boundary pH of 3 indicated acid buffering by K-feldspar dissolution. The processes identified in the incubation experiments were used to formulate a kinetic reaction modelling framework that was able to reproduce the major ion composition during subsequent column experiments. These experiments showed that there was at least 2 orders of magnitude difference between reaction rates of the incubation and column experiments. However, the combined approach was useful for identifying and quantifying key geochemical reactions that affect the water quality evolution in represented field conditions and will serve as basis for the model–based interpretation of the operational field scale injection and recovery experiment.**

Keywords: managed aquifer recharge, ASR, mineral kinetics, MAR

I. INTRODUCTION

The geochemical changes that will occur during the injection of reverse osmosis (RO) water into a deep pyritic aquifer are the direct result of the water-sediment interactions. These water-sediment interactions modify both, the aquifer matrix and the injectant composition. Therefore, understanding and quantifying these interactions is fundamental for an effective management of water resources, as they will control either the aimed quality improvement or the possible quality deterioration of the water recovered. This may impinge on the economic and technical feasibility of managed aquifer recharge (MAR) operations.

Upscaling of geochemical processes identified and quantified at the laboratory scale requires detailed process understanding to overcome the discrepancies expected due to greater physical and geochemical complexity in field scale systems [3]. Therefore, robust datasets from (controlled) experiments at different scales and the rigorous analyses of the underlying physical transport and reactive processes by numerical modeling are very important for gaining an adequate process understanding [4].

The present study aims at evaluating the application of a previously batch-experimentally derived reaction network [1, 2] to a column experiment for simulating the geochemical response of RO water injection into pyritic sediments of a deep anoxic aquifer in Perth, Western Australia.

II. MATERIALS AND METHODS

A. Target aquifer

The Leederville aquifer in Perth, Western Australia, is anoxic, NO_3–depleted, slightly brackish, and moderately to highly reducing. The sediments were deposited during alternating periods of continental, paralic and marine deposition, which have created a complex sedimentary sequence of interbedded sands, silts and shales.

B. Sediment material

Sediment material was collected between 107 and 255 m below ground level (mbgl) via diamond core drilling using a triple tube coring method to minimize core loss and mud invasion of the cores through the Leederville Formation. The barrels were split in a specifically designed anaerobic N_2-positive pressure chamber installed next to the drilling rig, which prevented oxidation of the sediments. The recovered sediment was stored in air-tight containers under N_2-atmosphere at 4°C until used.

The sediment in the targeted injection section of the aquifer (120 to 220 mbgl) consisted of interbedded sands, silts and clays [1]. In order to represent the flow through sandy layers of the aquifer, the sediment was firstly homogenized in an anaerobic chamber to provide sufficient material for the column experiments. Subsequently, the sediment was wet sieved (< 0.09 mm) to remove

approximately 1.5% of the finer sediment prior to the packing of the column. Quantitative XRD of the resultant sediment showed predominantly quartz (72%), K-feldspar (24%), with minor quantities of pyrite (2%) and Na-feldspar (2%). All other minerals were below analytical detection (<1%). Sediment organic matter (SOM) of 0.1 w/w% was determined by combustion and chromium reducible sulfur of 0.71 w/w% was measured.

C. Column experimetns

The laboratory soil stainless steel column was 2 m high and 14.5 cm internal diameter. The columns had 17 sampling ports (4mm i.d.) fitted 60mm into the centre of the column at 0, 4, 11, 18, 25, 32, 39, 46, 59, 75, 92, 109, 125, 142, 158, 175, and 192 cm from the base of the column. Outer ends contained a silicon septum allowing a hydrodermic syringe needle to be inserted for the removal of water samples for complete chemical analysis.

The columns were operated in a saturated up-flow mode with the effluent tubing passed through a peristaltic pump to regulate column flow at approximately 360 mL day^{-1}. This flow gave a linear velocity of approximately 5.2 cm day^{-1} and a water residence time of 39 days, in agreement with the aquifer groundwater velocities. To overcome an estimated high reductive capacity (890 µmol O_2 g^{-1}) under experimental low flow conditions [5], aerobic water was flushed through the columns at 21 L day^{-1} for 47 days in an attempt to further oxidize the sediment prior to the reduced flow conditions.

D. Reactive transport modelling

Incubation experiments on the target aquifer sediments and geochemical PHREEQC-2 [6] simulations have previously been performed to identify and quantify the major geochemical reactions responsible for the observed water quality changes while RO water is in contact with the sediments [1, 2]. The combined experimental and numerical modeling approach indicated that pyrite oxidation was the main oxygen reductant followed by sedimentary organic matter and Fe-carbonates (Reactions 1-3 in Table I). The pH and ion behaviour was subsequently controlled by dissolution rates of carbonates (Reaction 4-5 in Table I), and primary aluminosilicate minerals (Reaction 6-7 in Table I).

The developed reaction network was subsequently utilized for simulating the column experiment. Simuations have been performed with the MODFLOW/MT3DMS/PHREEQC-2 - based reactive multi-component transport model PHT3D [7].

TABLE I. CONTROLLING GEOCHEMICAL PROCESSES IDENTIFIED AND USED IN THE MODELLING OF AEROBIC EXPERIMENTS.

Reaction stoichiometry
(1) $FeS_2 + 3\ ¾\ O_2 + 3\ ½\ H_2O \rightarrow Fe(OH)_3 + 2\ SO_4^{2-} + 4\ H^+$
(2) $CH_2O + O_2 \rightarrow CO_2 + H_2O$
(3) $FeCO_3 + ¼\ O_2 + 1\ ½\ H_2O \rightarrow Fe(OH)_3 + CO_2$
(4) $FeS_2 + 3\ ¾\ O_2 + 1\ ½\ H_2O + 2\ CaCO_3 \rightarrow Fe(OH)_3 + 2\ Ca^{+2} + 2\ SO_4^{2-} + 2\ CO_2$
(5) $CaFe_{0.6}Mg_{0.4}(CO_3)_2 + 2\ H^+ \rightarrow Ca^{+2} + 0.6\ Fe^{+2} + 0.4\ Mg^{+2} + 2\ HCO_3^-$
(6) $KFe_3AlSi_3O_{10}(OH)_2 + 10\ ½\ H_2O + ¾\ O_2 + H^+ \rightarrow K^+ + 3\ Fe(OH)_3 + Al(OH)_3 + 3\ H_4SiO_4$
(7) $NaFe_3AlSi_3O_{10}(OH)_2 + 10\ ½\ H_2O + ¾\ O_2 + H^+ \rightarrow Na^+ + 3\ Fe(OH)_3 + Al(OH)_3 + 3\ H_4SiO_4$

In contrast to the ultra-pure water used in the batch experiments, the injectant composition included nitrate, therefore the reaction rate expression of pyrite oxidation by molecular oxygen was further extended as:

$$FeS_2 + 3NO_3 + 2H_2O \rightarrow Fe(OH)_3 + 2SO_4 + 1.5N_2 + H^+$$

and included in the reaction network based on the applied rate expression [8]:

$$r_{pyr} = \left(C_{O_2}{}^{0.5} + f_2 C_{NO_3}{}^{-0.5}\right) C_{H^+}{}^{-0.11} \left(10^{-10.19}\frac{A_{pyr}}{V}\right)\left(\frac{C}{C_0}\right)_{pyr}^{0.67}\left(1-\left(\frac{IAP}{K}\right)\right)_{pyr}$$

where r_{pyr} is the specific oxidation rate for pyrite, C_{O_2}, C_{NO_3} and C_{H^+} are the aqueous dissolved oxygen (DO), nitrate and proton concentrations. The term (A_{pyr}/V) is the ratio of mineral surface area to solution volume, (C/C_0) is a factor to account for changes in A_{pyr} resulting from the successively progressing reaction, and (IAP/K) is the saturation ratio. f_2 is a constant, which based on previous studies was assumed to be unity [8].

Aerobic SOM oxidation (represented as carbohydrate and assumed to be equivalent to TOC concentrations) contributed to a variable O_2 consumption [1].

Similarly, the kinetic reaction rate expression was extended for the oxidation of SOM by oxygen, nitrate and sulfate based on the Monod-type rate expression [6]:

$$r_{DOC} = \left[k_{O_2}\frac{C_{O_2}}{2.94\times10^{-4}+C_{O_2}} + 2\times10^{-12}\frac{C_{NO_3^-}}{1.55\times10^{-4}+C_{NO_3^-}} + 1\times10^{-13}\frac{C_{SO_4^{2-}}}{1.0\times10^{-4}+C_{SO_4^{2-}}}\right]$$

where r_{DOC} is the overall degradation rate of organic matter, $kO_2$is the rate constants of carbon mineralisation under aerobic conditions. The rate constants under denitrifying and sulphate-reducing conditions were fixed to previously reported values [6]. The terms C_{O_2}, C_{NO_3}, and C_{SO_4} are the aqueous concentrations of oxygen, nitrate and sulphate.

The weathering of aluminosilicates, mainly K-feldspars ($KAlSi_3O_8$) and albite ($NaAlSi_3O_8$) minerals was described by the generalized equation proposed by [9]. The Fe(II)-carbonates phase identified (ankerite), also competed for oxygen and was included in the model with a representing formula of $CaFe_{0.6}Mg_{0.4}(CO_3)_2$ with log K=-17.40 [1]. The

dissolution rate expression for ankerite was simulated as described in [10]. The inclusion of these phases' kinetic rate expressions in the reactive model are detailed in [2]. The rate of calcite dissolution was numerically included in the model as proposed by [11], and scripted in the standard PHREEEQC-2 database.

Fe- and Al-oxides precipitation/dissolution were assumed to be kinetically controlled based on the calculated saturation ratios. Sorption was considered through cation exchange reactions and surface complexation. Initial concentrations assumed that the ion exchange sites were in equilibrium with the average ambient groundwater composition at the measured CEC (Table II).

TABLE II. INITIAL MINERAL CONCENTRATIONS AND EQUILIBRATED INITIAL EXCHANGER COMPOSITIONS.

Minerals	**mol L_w^{-1*}**	**Cations**	**mol L^{-1}**
Pyrite	5.8×10^{-2}	Ca-X2	9.5×10^{-5}
K-feldspar	2.1	Mg-X2	2.4×10^{-5}
Albite	1.8×10^{-1}	Mn-X2	1.8×10^{-8}
Calcite	2.4×10^{-2}	Na-X	1.2×10^{-5}
Magnesite	8.0×10^{-3}	K-X	1.5×10^{-6}
Ankerite	1.2×10^{-1}	Fe-X2	2.9×10^{-18}
Gypsum	1.0×10^{-2}	AlOH-X2	5.8×10^{-11}
Ferrihidrate	0	H-X	1.5×10^{-8}
Gibbsite	0		

*moles per litre water

III. MODEL-BASED INTERPRETATION OF THE CHEMICAL CHANGES IN THE COLUMN

A. Oxidation processes

The calibrated model simulations compared to the observed aqueous concentrations along the column are presented in Figure 1. The model corroborated oxygen consumption by SOM and pyrite at the entrance of the column, whilst nitrate was able to enter the column to around 0.25m and then be simultaneously reduced by pyrite and SOM. The model results represent well the depletion in oxygen and nitrate measured, accompanied by a sulphate increase due to pyrite oxidation. The pH was lowered by the release of CO_2 forming carbonic acid and the simultaneous release of Fe^{2+} further oxidized in the presence of O_2 and NO_3 and subsequently precipitated as ferrihydrate, contributing to proton release by:

$$Fe^{3+} + 3\ H_2O \rightarrow Fe(OH)_3 + 3\ H^+$$

This proton generation was followed by carbonate dissolution, which consisted to a minor fraction of highly reactive carbonates (calcite) and ankerite. The stoichiometric molal correlation between aqueous concentrations of Ca and Mg ($R^2 = 0.98$) with a ratio of Ca/Mg = 0.3. The strong linear correlation between Ca and Mg with HCO_3 ($R^2 = 0.98$) at a ratio of 2:1is in agreement with carbonate dissolution and bicarbonate production at a pH of 8 by carbonate buffered pyrite oxidation or aggressive dissolution of carbonate minerals due to the low ionic strength of the influent RO water [12].

The dissolution of K-feldspar was well represented by the reaction network and constrained by the K^+ concentrations. Initially faster dissolution rates occurred when O_2 was still present, but this was followed by a constant dissolution rate along the anoxic part of the column. On the other hand, albite dissolution occurred at negligible rate with no contribution to Na^+ concentrations in the column water.

B. Oxygen depleted zone

Once the oxygen and nitrate were consumed, Fe and Al concentrations above analytical detection limits were measured. Both, Fe- and Al-hydroxides precipitated completely under aerobic denitrifying conditions. Under anoxic reducing conditions Al concentrations were sourced from the continuous dissolution of aluminosilicates and these concentrations were well represented by the model (Figure 1). The model-based interpretation indicated that aqueous concentrations of Fe^{2+} were sourced from the reductive dissolution iron oxides by organic matter.

C. Trace metal release and sorption

Reference [1] suggested the release of heavy metal(loid)s as a result of pyrite oxidation due to the strong linear relationships within sediment trace metal concentrations and pyrite. The stoichiometric release resulted in negligible concentrations (i.e., below analytical detection limits) of Cd, Co, Cr, Cu, Ni, Pb and Zn most likely due to sorption onto ferrihydrite minerals created from the oxidation of pyrite. The stoichiometric release ratio of $1x10^{-3}$ Mn^{+2} to one mol of FeS_2 dissolved satisfactorily represented the aqueous concentrations in the column (Figure 1). The model results showed oversaturation of Mn-carbonate minerals and the allowance of rhodochrosite precipitation explained the decrease in Mn^{+2} concentrations in the oxygen depleted zone.

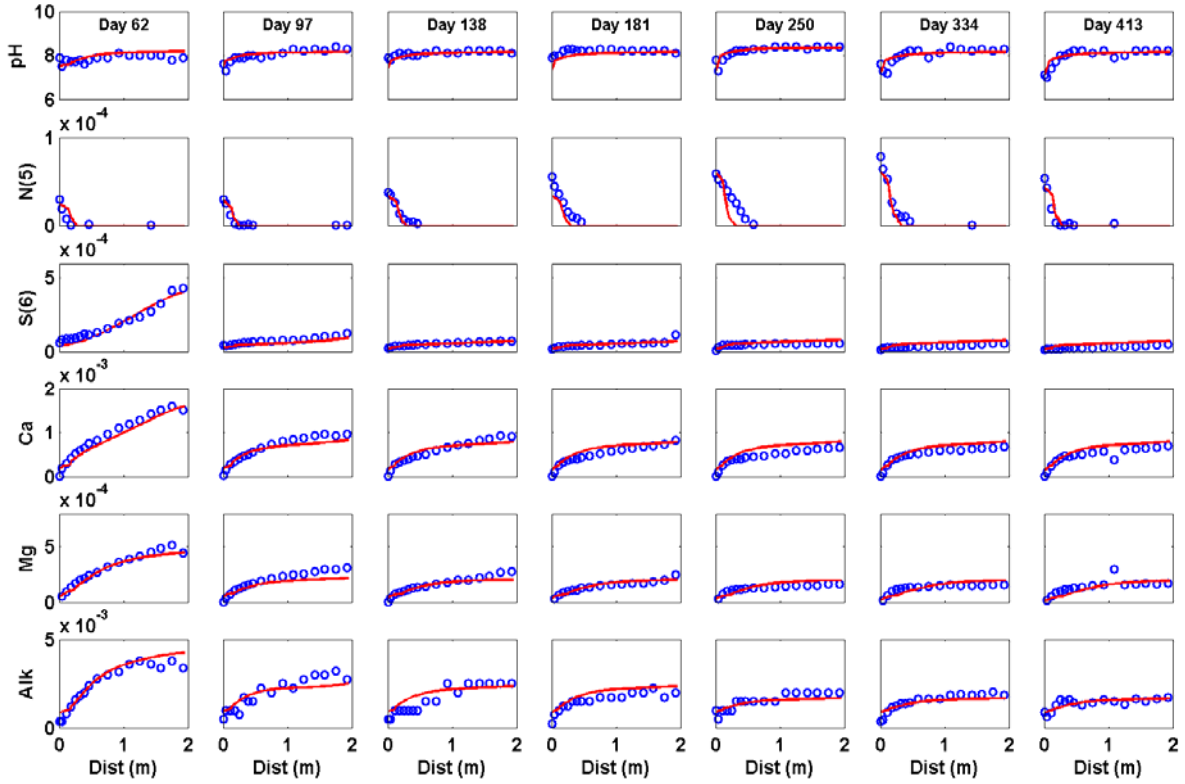

Figure 1. Observed and simulated concentration profiles at 63, 98, 138, 181, 250, 334, and 413 days. Measured concentrations (symbols) and simulation calibrated model results of rate constants upscaling from batchexperiments (red line) expressed in moles L^{-1} of bulk volume.

IV. Mineral Kinetic Weathering Rates

Pyrite dissolution under aerobic-denitrifying conditions occurred between 0 and 0.5 m, and the optimised weathering rates ranged from $1.4x10^{-11}$ to $1.6x10^{-9}$ mol/L/s, and averaged $1.7x10^{-11}$ mol/L/s. This is an equivalent average concentration-normalised pyrite oxidation rate of $2.4x10^{-12}$ mol/g/s, which is around two-orders of magnitude slower than determined concentration-normalised pyrite oxidation rate in batch experiments.

The optimised normalised K-feldspar weathering rate determined in the calibrated model was $2.6x10^{-14}$ mol/g/s, which was around 1.97 orders of magnitude slower than pyrite in agreement with the relative difference found during incubation experiments (Table III). Albite weathering rates were not considered due to its negligible contribution.

Calcite dissolution mainly occurred as buffering to the acidity produced by pyrite oxidation followed by continuous dissolution of Fe(II)-carbonates in the oxygen depleted zone of the column. The fastest dissolution of calcite was observed at the entrance of the column, at $7.6x10^{-10}$ mol/L/s decreasing to $1.2x10^{-9}$ mol/L/s until saturation was reached. The calibrated numerical model indicated a normalised-concentration weathering rate of calcite of approximately $9.6x10^{-11}$ mol/g/s. Although in the same order of magnitude, the 1.6 orders of magnitude faster dissolution rate of calcite than pyrite was close to the 0.8 average orders of magnitude difference determined by [2]. Ankerite dissolution rate remained almost steady at $9.2x10^{-11}$ mol/L/sfrom the oxidation to reducing zone of the column. The optimised average normalised-concentration weathering rate of approximately $3.4x10^{-12}$ mol/g/s, almost 1.5 orders of magnitude slower than calcite, is in agreement with the rate difference of 1.6 orders of magnitude previously determined by [1].

A. *Reactive mineral surface areas*

The model results suggested that pyrite surface area per gram of mineral was ~0.26 m^2/g. This value is consistent with the previous pyrite reactive surface area determined during the incubation experiments (0.1-0.2 m^2/g), and supported the preliminary assumptions of a uniform pyrite grain size across lithologies. Furthermore, the optimised reaction rate parameters, specifically the (A/V) values determined for K-feldspar, calcite and ankerite, reflected the low surface area per gram of mineral in the column resulting from the sieving of the fine grained sediment fraction. Average K-feldspar reactive surface area determined from the calibrated model was 1.2 m^2/g, ten times smaller than average sand reactive surface area determined from the incubation experiments. Similarly, reactive surface areas for calcite and ankerite were 0.001 and 0.63 m^2/g, which are closer to the lower end carbonate surface areas determined for the clay samples in the incubations. The latter indicates

that although most of the fine sized aluminosilicate and carbonate minerals were sieved out from the column, the weathering reaction rates depended on the other reactive minerals present, hence the consistency in relative differences between mineral reaction rates from the incubation and the column experiments.

TABLE III. AVERAGE NORMALISED-CONCENTRATION WEATHERING RATES, (A/V), AND COMPARISON WITH INCUBATION EXPERIMENTS.

Minerals	Average batch results					Column results					
	Content		*Weathering rate*	*(A/V)*	*Relative difference*	*Content*		*(A/V)*	*surface area*	*Weathering rate*	*Relative difference*
	wt%	*g/L*	*mol/g/s*	*m^2/L*	*(-)*	*wt%*	*g/L*	*m^2/L*	*m2/g*	*mol/g/s*	*(-)*
Pyrite	0.60	0.90	1.15E-10	0.20	0.00	0.29	6.96	1.78	0.26	2.40E-12	0.00
K-feldspar	26.6	39.9	2.12E-12	3300	-1.70	24.0	576	700	1.22	2.60E-14	-1.97
Albite	2.05	3.08	1.66E-11	434	-0.80	-	-	-	-	-	-
Calcite	0.01	0.02	7.06E-10	0.10	0.80	0.10	2.40	0.01	0.004	9.60E-11	1.60
Ankerite*	0.12	0.18	1.63E-11	1.57	-1.60	0.50	12.0	15.0	1.25	3.40E-12	-1.45

[1]realtive difference in rates normalised to pyrite weathering rate. Ankerite's relative difference with respect to calcite.

V. IMPLICATIONS

This study demonstrated that sediment incubations identified the key reactions, which enabled estimation of in-situ rates of competing redox and buffering reactions that prevailed within the different lithological units of a heterogeneous aquifer. Up to 2-orders of magnitude difference in reaction rates were determined from batch to column scale experiments, which are more likely representing field conditions. However, the direct translation of water-sediment ratios from batch experiments to the large-scale column experiments for the driving reaction of pyrite oxidation followed by the inclusion of the relative differences in reaction rates supported a comprehensive model-based interpretation of the geochemical changes along the column. The model built included the complex interplay of the geochemical processes that occur under the transition from an aerobic to an anaerobic environment. The simulations confirmed that organic matter and pyrite oxidation were the main sinks of O_2, and their direct effect on the acidification produced was responsible for the subsequent dissolution of carbonate and feldspar minerals. The model-based interpretation and quantification of the key-reactions occurring in the here investigated column experiment will serve as a starting point for the field-scale ASR reactive transport modeling.

ACKNOWLEDGMENT

This research was funded by the Water Foundation and Water Corporation of Western Australia.

REFERENCES

[1] Descourvieres, C.; Hartog, N.; Patterson, B. M.; Oldham, C.; Prommer, H., Geochemical controls on sediment reactivity and buffering processes in a heterogeneous aquifer. Appl. Geochem. 2010, 25, (2), 261-275.

[2] Descourvieres, C.; Prommer, H.; Oldham, C.; Greskowiak, J.; Hartog, N., Kinetic Reaction Modeling Framework for Identifying and Quantifying Reductant Reactivity in Heterogeneous Aquifer Sediments. Environ. Sci. Technol. 2010, 44, (17), 6698-6705.

[3] Strömberg, B.; Banwart, S., Weathering kinetics of waste rock from the Aitik copper mine, Sweden: scale dependent rate factors and pH controls in large column experiments. J. Contam. Hydrol. 1999, 39, (1-2), 59-89.

[4] Appelo, C. A. J.; Verweij, E.; Schafer, H., A hydrogeochemical transport model for an oxidation experiment with pyrite/calcite/exchangers/organic matter containing sand. Appl. Geochem. 1998, 13, (2), 257-268.

[5] Patterson, B. M.; Shackleton, M.; Furness, A. J.; Pearce, J.; Descourvieres, C.; Linge, K. L.; Busetti, F.; Spadek, T., Fate of nine recycled water trace organic contaminants and metal (loid) s during managed aquifer recharge into a anaerobic aquifer: Column studies. Water Res. 2009.

[6] Parkhurst, D. L.; Appelo, C. A. J. User's guide to PHREEQC (Version 2) -- A computer program for speciation, reaction-path, advective-transport and inverse geochemical calculations; U.S. Geological Survey: Reston, VA, 1999.

[7] Prommer, H.; Barry, D. A.; Zheng, C., MODFLOW/MT3DMS-based reactive multicomponent transport modeling. Ground Water 2003, 41, (2), 247-257.

[8] Eckert, P.; Appelo, C. A. J., Hydrogeochemical modeling of enhanced benzene, toluene, ethylbenzene, xylene (BTEX) remediation with nitrate. Water Resour. Res. 2002, 38, (8), 1130.

[9] Sverdrup, H.; Warfvinge, P., Estimating field weathering rates using laboratory kinetics. Rev. Mineral. Geochem. 1995, 31, (1), 485-541.

[10] Chou, L. E. I.; Garrels, R. M.; Wollast, R., Comparative study of the kinetics and mechanisms of dissolution of carbonate minerals. Chem. Geol. 1989, 78, (3-4), 269-282.

[11] Plummer, L. N.; Wigley, T. M. L.; Parkhurst, D. L., The kinetics of calcite dissolution in CO2-water systems at 5º to 60ºC and 0. 0 to 1. 0 atm CO2. Am. J. Sci. 1978, 278, 179-216.

[12] Johnson, J.; Baker, L.; Fox, P., Geochemical transformations during artificial groundwater recharge: soil-water interactions of inorganic constituents. Water Res. 1999, 33, (1), 196-206.